Detection of incipient faults in nine-phase machines: impact of the star winding configuration

Anthony El Hajj[a,b,*], Eric Semail[a], Abdelmounaim Tounzi[a], Darius Vizireanu[b], Jalal Cheaytani[b]

[a]*Univ. Lille, Arts et Metiers Institute of Technology HESAM Universite, Centrale Lille, Junia, ULR 2697 - L2EP, Lille, 59000, France*
[b]*EDF R&D, Palaiseau, 91120, France*

Abstract

Two approaches are commonly used for modelling and control of nine-phase (triple star) fault-tolerant machines with symmetrical and asymmetrical star winding configurations: The Vector Space Decomposition (VSD) and the decentralized d-q modelling. In this paper, it will be shown how the VSD approach used for machines with an Asymmetrical Star Winding Configuration (ASWC), unlike the decentralized d-q one used for machines with a Symmetrical Star Winding Configuration (SSWC), can be helpful for non-intrusive Fault Detection and Diagnosis (FDD) purposes. Supporting MATLAB/Simulink simulations are discussed.

Keywords: multiphase permanent-magnet synchronous machines, fault detection, vector space decomposition, decentralized d-q modelling, symmetrical and asymmetrical star winding configurations

1. Introduction

During the last decade, the use of multiphase Permanent-Magnet Synchronous Machines (PMSMs) has become more and more common in several domains including wind energy conversion. These machines have been gaining interest due to their high torque/power density, good efficiency with a variable speed, and fault tolerance leading to a higher functional reliability. Furthermore, in the case of wind energy conversion, they are mainly used at variable speed connected to the

---

*Corresponding author

Email addresses: `anthony.el-hajj@edf.fr` (Anthony El Hajj), `Eric.SEMAIL@ENSAM.EU` (Eric Semail), `abdelmounaim.tounzi@univ-lille.fr` (Abdelmounaim Tounzi), `darius.vizireanu@edf.fr` (Darius Vizireanu), `jalal.cheaytani@edf.fr` (Jalal Cheaytani)

grid through converters and as direct-driven machines thus avoiding problems of the mechanical gearbox [1].

However, a multiphase PMSM, like any other machine, is prone to faults: stator faults (inter-turn short circuits, increased resistance connection) and/or rotor faults (demagnetization of permanent magnets, eccentricity, bearings, etc). The fault tolerance and the robustness with respect to incipient faults require nevertheless a detection of such defects in early stages to avoid any severe damage, to reconfigure the control, and to organize maintenance schedule. In this aim, several research works are conducted to find the most relevant indicators [2–6]. Most studies dealt with 3-phase PMSMs. However, there are some differences between the mathematical properties of 3-phase machines and multiphase ones that turn out to be useful for control [7–9] and Fault Detection and Diagnosis (FDD) of multiphase machines [10].

Two approaches are mainly used for modelling and control of multi-three-phase machines: the VSD that is used for any number of phases [7, 9, 11], and the decentralized d-q modelling, used only when the number of phases is a multiple of 3 [12, 13]. In this paper, it will be shown how the VSD, unlike the decentralized d-q modelling, can also be used for FDD purposes in the case of a 9-phase PMSM with an asymmetrical star winding configuration. More precisely, it will be shown how the projection of non-intrusive quantities (such as stator currents) onto the space defined by the Concordia transform with the VSD approach can be helpful for FDD. Indeed, both Concordia transforms, the one with the d-q modelling approach and the one with the VSD approach, define orthonormal subspaces but with different harmonic properties. With the decentralized d-q modelling approach, the Concordia transform defines several subspaces containing each the 1st order harmonic with quite the same amplitude in both healthy and faulty states. However, with the VSD approach, the Concordia transform defines several subspaces of which only one subspace contains the 1st order harmonic in the healthy state. Therefore, the emergence of this harmonic in the remaining subspaces in the faulty state can be very useful for FDD. These mathematical properties and the differences between the healthy state and a faulty case (increase of resistance connection) are studied in details in this paper. To the best of the author's knowledge, these differences have not yet been studied in the literature.

The rest of the paper is organized as follows. In Section 2, the different types of multiphase machines and their modelling are introduced. In Section 3, the effects of the same fault on two 9-phase PMSMs, one with a symmetrical star winding configuration (SSWC) and the other with an asymmetrical star configuration (ASWC), are compared. Conclusions and future works are provided in Section 4.

2. Types of multiphase machines and their modelling

2.1. Types of multiphase machines

Depending on the applications, the number of phases of a multiphase machine may vary. There are mainly two categories of multiphase machines [9, 11]:

- Machines with a prime number of phases (5, 7, 11, etc.). All phases are often connected to one neutral.

- Machines whose number of phases is a multiple of 3. The multiple three-phase star aspect of these machines might be interesting for industrials. Each three windings that are separated by $120°$ or $240°$ constitute a three-phase star, usually with one isolated neutral per star. If a fault occurs on one phase, the whole star to which the faulty phase belongs should be isolated. For these machines, there are symmetrical and asymmetrical star winding configurations (Figure 1). The asymmetrical configuration, ASWC, corresponds to the case where the stars are phase-shifted by an angle γ in the electrical space. The symmetrical configuration, SSWC, corresponds to the case where the stars are not phase-shifted.

In this paper, two 9-phase PMSMs are studied: the first one is a 30-pole PMSM with a SSWC and the second one is a 32-pole PMSM with an ASWC (Figure 1). For both machines, 3 stars with 3 isolated neutrals are considered.
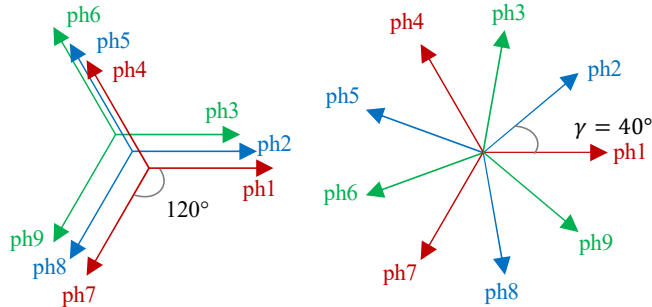

Figure 1: Phase distribution of both 9-phase machines: SSWC (on the left) and ASWC (on the right)

2.2. VSD and decentralized d-q modelling

As introduced previously, two approaches can be used for the modelling and control of multiphase machines: the VSD and the decentralized d-q modelling. The former approach is a general one, it can be used whether the number of phases is a multiple of 3 or not [11]. In the absence of reluctance effect and with regular manufacturing for the stator, the inductance matrix in the new space is then diagonal

and there is no need to consider cross-couplings between the different subspaces. The latter approach, i.e. the decentralized d-q modelling, is used only when the number of phases is a multiple of 3. Note that depending on the machine winding arrangement, the magnetic coupling between phases belonging to two different stars can or cannot be neglected. Cross-couplings should therefore be considered between the different subspaces to provide an adequate modelling.

For both modelling methods, a Concordia transform matrix $\boldsymbol{C_n}$ (n being the total number of phases) that allows the projection of a vector quantity $\boldsymbol{g_n}$ (such as current or voltage) from the initial space onto a new space is defined, it gives $\boldsymbol{g_{\alpha\beta 0}}$

$$\boldsymbol{g_{\alpha\beta 0}} = \boldsymbol{C_n} \cdot \boldsymbol{g_n}, \boldsymbol{g_n} = \begin{pmatrix} g_1 & g_2 & ... & g_n \end{pmatrix}^T \tag{1}$$

In the decentralized d-q approach, there are $\frac{n}{3}$ two-dimensional subspaces $(\alpha_j, \beta_j), j \in \left\{1, 2, ..., \frac{n}{3}\right\}$ and $\frac{n}{3}$ one-dimensional (zero-sequence) subspaces 0_j, one (α_j, β_j) and one 0_j per three-phase star. Each (α_j, β_j) mainly contains the 1st order harmonic in the healthy state. Other harmonics appear in the faulty state. The value of the 1st order harmonic being very high compared to the other harmonics, the disturbance generated by the fault in these subspaces is very small.

In the case of the 9-phase machine with a SSWC studied in this paper, the mutual inductances between the different phases are negligible (8 % of the self-inductance at most). The Concordia transform matrix (2) can therefore be written in a simple manner as the concatenation of three diagonal blocks of the 3-phase Concordia transform (the machine is considered as three independent stars)

$$\boldsymbol{C_n} = \boldsymbol{C_{9_{sym}}} = \begin{pmatrix} \boldsymbol{C_3} & \boldsymbol{0_{3*3}} & \boldsymbol{0_{3*3}} \\ \boldsymbol{0_{3*3}} & \boldsymbol{C_3} & \boldsymbol{0_{3*3}} \\ \boldsymbol{0_{3*3}} & \boldsymbol{0_{3*3}} & \boldsymbol{C_3} \end{pmatrix},$$

$$\boldsymbol{C_3} = \sqrt{\frac{2}{3}} \begin{pmatrix} 1 & \cos 120° & \cos 240° \\ 0 & \sin 120° & \sin 240° \\ \frac{1}{\sqrt{2}} & \frac{1}{\sqrt{2}} & \frac{1}{\sqrt{2}} \end{pmatrix} \tag{2}$$

$$\boldsymbol{g_{\alpha\beta 0}} = \begin{pmatrix} g_{\alpha 1} & g_{\beta 1} & g_{01} & g_{\alpha 2} & g_{\beta 2} & g_{02} & g_{\alpha 3} & g_{\beta 3} & g_{03} \end{pmatrix}^T \tag{3}$$

$$\begin{pmatrix} g_1 \\ g_4 \\ g_7 \end{pmatrix} = \begin{pmatrix} g_2 \\ g_5 \\ g_8 \end{pmatrix} = \begin{pmatrix} g_3 \\ g_6 \\ g_9 \end{pmatrix} = \begin{pmatrix} g \cdot \sin\theta_e \\ g \cdot \sin(\theta_e - 120°) \\ g \cdot \sin(\theta_e - 240°) \end{pmatrix} \tag{4}$$

The harmonics mapping of this machine, in the healthy state, is given in Table 1. It shows that each of the subspaces (α_1, β_1), (α_2, β_2), and (α_3, β_3) contains mainly the 1st order harmonic.

Table 1: Harmonics mapping of the machine with a SSWC, healthy state	
Subspace	Harmonics
(α_1, β_1)	1, 5, 7, 11, etc.
(α_2, β_2)	1, 5, 7, 11, etc.
(α_3, β_3)	1, 5, 7, 11, etc.
$0_1, 0_2, 0_3$	3, 9, 15, etc.

Table 2: Harmonics mapping of the machine with an ASWC, healthy state	
Subspace	Harmonics
(α_1, β_1)	1, 17, 19, etc.
(α_2, β_2)	7, 11, 25, etc.
(α_3, β_3)	3, 15, 21, etc.
(α_4, β_4)	5, 13, 23, etc.
0	9, 18, 27, etc.

In the VSD approach, there are $\frac{n-1}{2}$ $(\alpha_j, \beta_j), j \in \left\{1, 2, ..., \frac{n-1}{2}\right\}$ subspaces (planes) and one zero-sequence subspace (line) if n is odd. There are $\frac{n-2}{2}$ $(\alpha_j, \beta_j), j \in \left\{1, 2, ..., \frac{n-2}{2}\right\}$ planes and two zero-sequence lines if n is even [8].

In the case of the 9-phase machine with an ASWC studied in this paper, there are 4 (α_j, β_j) and one zero-sequence subspace 0. The harmonics mapping of this machine is summarized in Table 2. (α_1, β_1) mainly contains the 1st order harmonic, (α_2, β_2) the 7th one, (α_3, β_3) the 3rd one, (α_4, β_4) the 5th one, and the zero-sequence subspace (0) the 9th one. The corresponding Concordia transform matrix ($\gamma = 40°$) is defined below (5) [11]

$$C_n = C_{9_{asym}} = \sqrt{\frac{2}{9}} \begin{pmatrix} 1 & \cos\gamma & \cos 2\gamma & \cos 3\gamma & ... & \cos 8\gamma \\ 0 & \sin\gamma & \sin 2\gamma & \sin 3\gamma & ... & \sin 8\gamma \\ 1 & \cos 2\gamma & \cos 2(2\gamma) & \cos 2(3\gamma) & ... & \cos 2(8\gamma) \\ 0 & \sin 2\gamma & \sin 2(2\gamma) & \sin 2(3\gamma) & ... & \sin 2(8\gamma) \\ 1 & \cos 3\gamma & \cos 3(2\gamma) & \cos 3(3\gamma) & ... & \cos 3(8\gamma) \\ 0 & \sin 3\gamma & \sin 3(2\gamma) & \sin 3(3\gamma) & ... & \sin 3(8\gamma) \\ 1 & \cos 4\gamma & \cos 4(2\gamma) & \cos 4(3\gamma) & ... & \cos 4(8\gamma) \\ 0 & \sin 4\gamma & \sin 4(2\gamma) & \sin 4(3\gamma) & ... & \sin 4(8\gamma) \\ \frac{1}{\sqrt{2}} & \frac{1}{\sqrt{2}} & \frac{1}{\sqrt{2}} & \frac{1}{\sqrt{2}} & ... & \frac{1}{\sqrt{2}} \end{pmatrix} \tag{5}$$

$$\boldsymbol{g_{\alpha\beta0}} = \begin{pmatrix} g_{\alpha1} & g_{\beta1} & g_{\alpha2} & g_{\beta2} & g_{\alpha3} & g_{\beta3} & g_{\alpha4} & g_{\beta4} & g_0 \end{pmatrix}^T \tag{6}$$

$$g_j = g \cdot \sin(\theta_e - (j-1) \cdot \gamma), j \in \{1, 2, ..., 9\} \tag{7}$$

The torque being generally generated by the 1st order harmonic, the currents in $(\alpha_j, \beta_j), j \in \{2, 3, 4\}$ are null in the healthy state, when $\boldsymbol{g_n}$ is balanced. In a faulty state, $\boldsymbol{g_n}$ is no more balanced and the 1st order harmonic appears in these subspaces. The changes are more significant than those in (α_1, β_1) or those in

the $(\alpha_j, \beta_j), j \in \{1, 2, 3\}$ subspaces of the decentralized d-q approach. It will be shown that these changes are relevant indicators for fault detection in multiphase machines.

Based on the considerations introduced above, the changes in the phase currents projected onto $(\alpha, \beta, 0)$ for a five-phase machine were used to identify Voltage Source Inverter (VSI) open-switch faults in [10]. In the following section, the same approach is considered for internal machine faults.

3. Simulation results

To show the effectiveness of the proposed approach, simulations are carried out in MATLAB/Simulink for both multiphase machines studied in healthy and faulty cases. Both machines, whose main characteristics are given in Table 3, are with tooth-concentrated windings and surface-mounted permanent magnets. Therefore, the values of the mutual inductances are low. Furthermore, to perform the simulations, some conditions and assumptions are made. They are listed hereafter:

- The machines are represented by equivalent-circuit models
- Saturation effects are neglected
- The neutrals of the 3 stars are isolated from each other
- The machines are controlled by VSIs
- The 'IGBT/Diode' block from Simscape is used to model the different switches of the VSIs
- A Field-Oriented Control (FOC) with Maximum Torque Per Ampere (MTPA) strategy is applied
- The switching frequency is: $f_{PWM} = 10$ kHz
- The simulations are done for the generator operating mode
- The DC bus voltage is constant, $V_{DC} = 650$ V

A general control diagram is shown in Figure 2. As discussed in Section 2, there are 3 (α_j, β_j) subspaces for the machine with a SSWC, each containing the 1st order harmonic (Table 1). A rotation of θ_e is applied to each (α_j, β_j) and the rotating subspaces $(d_j, q_j), j \in \{1, 2, 3\}$ are obtained. There are therefore 6 PI controllers (d_1, q_1, d_2, q_2, d_3, and q_3) in the control loop of the first machine. This corresponds to a decentralized d-q control strategy. On the other hand, there are 4 (α_j, β_j) subspaces for the machine with an ASWC, containing mainly the 1st, 7th, 3rd, and 5th order harmonics respectively (Table 2). Rotations of θ_e, $7\theta_e$, $3\theta_e$, and $5\theta_e$ are applied to (α_1, β_1), (α_2, β_2), (α_3, β_3), and (α_4, β_4) respectively and the
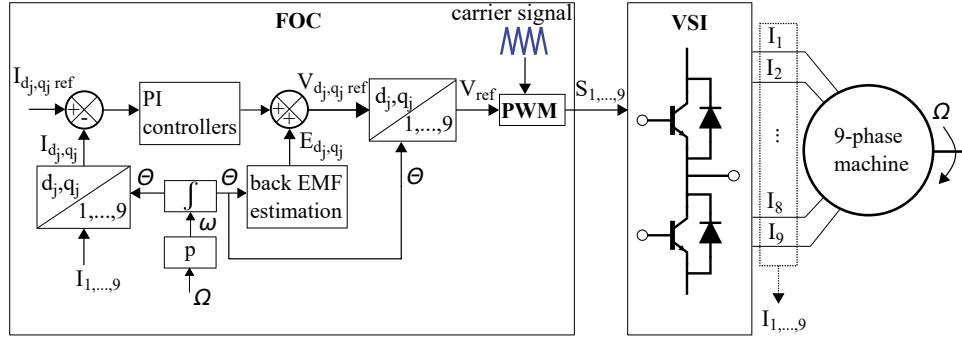
Figure 2: Current-control loop of a 9-phase PMSM based on Field-Oriented Control or FOC technique: $j \in \{1, 2, 3\}$ for the symmetrical machine and $j \in \{1, 2, 3, 4\}$ for the asymmetrical one

rotating subspaces $(d_j, q_j), j \in \{1, 2, 3, 4\}$ are obtained. There are therefore 8 PI controllers in the control loop of the second machine. This corresponds to a VSD control strategy.

Table 3: Parameters of both machines

Parameter	Machine with a SSWC	Machine with an ASWC
Slots/Poles	36/30	36/32
Number of phases	9	9
Phase winding resistance R_s	57 mΩ	33 mΩ
Rated voltage (V)	335	335
Rated power (kW)	55	55
Rotation speed (rpm)	200	187.5
Frequency (Hz)	50	50
Torque (N.m)	2780	2780

One of the easiest faults to model is the increase of resistance connection. The stator resistance value of one phase (or several phases) is increased. This fault is common in electric machines. It can occur in any power connection. If not detected at its incipient stage, it leads to local excessive heating and increases losses [6, 14, 15].
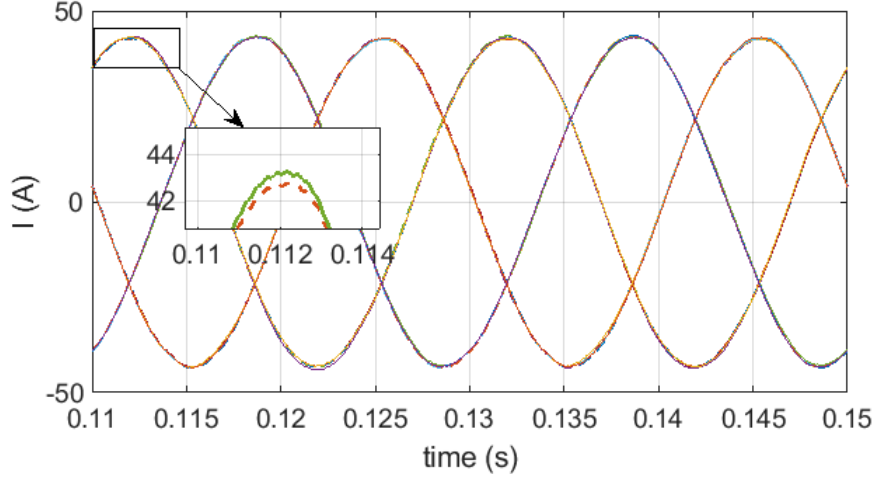
Figure 3: (Machine with a SSWC) 9 stator currents versus time in healthy (dashed lines) and faulty (solid lines, $R_{add} = 0.1\Omega$) states

3.1. Comparison of currents in healthy and faulty states

Figure 3 shows the steady-state phase currents versus time plots when a resistor $R_{add} = 0.1\Omega \approx 2R_s$ is added to phase 1 of the machine with a SSWC at rated speed/power conditions. Figure 4 shows $i_{\beta_j} = f(i_{\alpha_j}), j \in \{1, 2, 3\}$ and $i_{\alpha_1} = f(t)$. The changes between healthy and faulty states are insignificant (less than 1%). This is due to the fact that the 1st order harmonic current is projected onto each $(\alpha_j, \beta_j), j \in \{1, 2, 3\}$ in both healthy and faulty states with quite the same amplitude. Therefore, the detection of incipient imbalance in the working space defined by the considered transformation $C_{9_{sym}}$ (2) appears as difficult.

Figure 5 depicts the steady-state phase currents versus time plots when a resistor $R_{add} = 0.1\Omega \approx 3R_s$ is added to phase 1 of the machine with an ASWC at rated speed/power conditions. For the currents, the differences in this natural space are slightly higher than in the previous case (30-pole machine). The currents are higher or lower in the healthy state than in the faulty state. It depends on the fault location and the mutual inductances between the faulty phase and the remaining healthy ones.
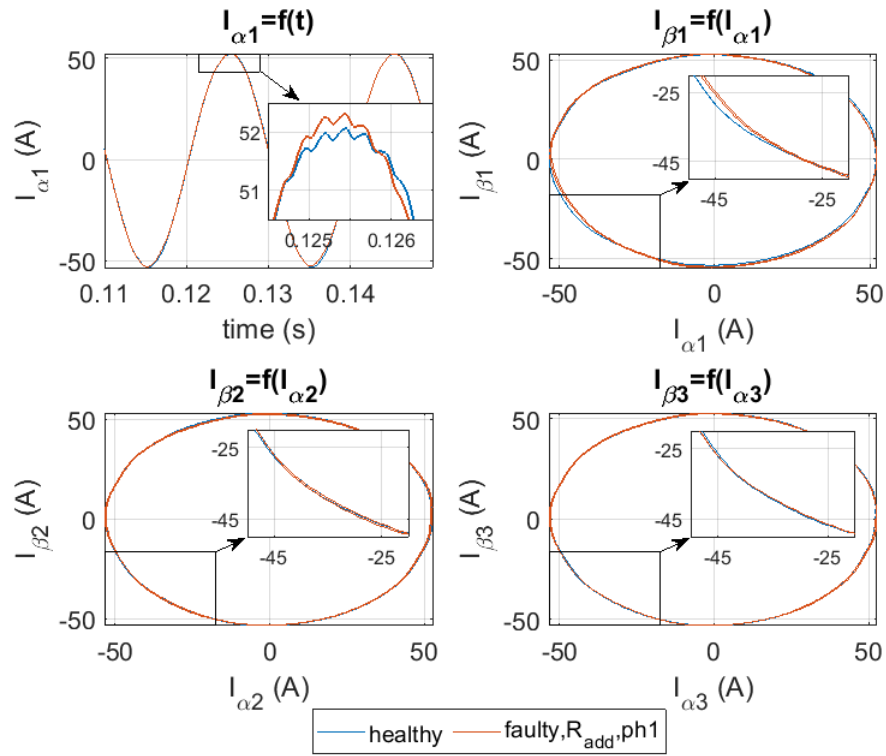
Figure 4: (Machine with a SSWC) Comparison of stator currents in $(\alpha_j, \beta_j), j \in \{1, 2, 3\}$ subspaces in healthy and faulty ($R_{add} = 0.1\Omega$) states: $I_{\alpha_1} = f(t)$ and $I_\beta = f(I_\alpha)$
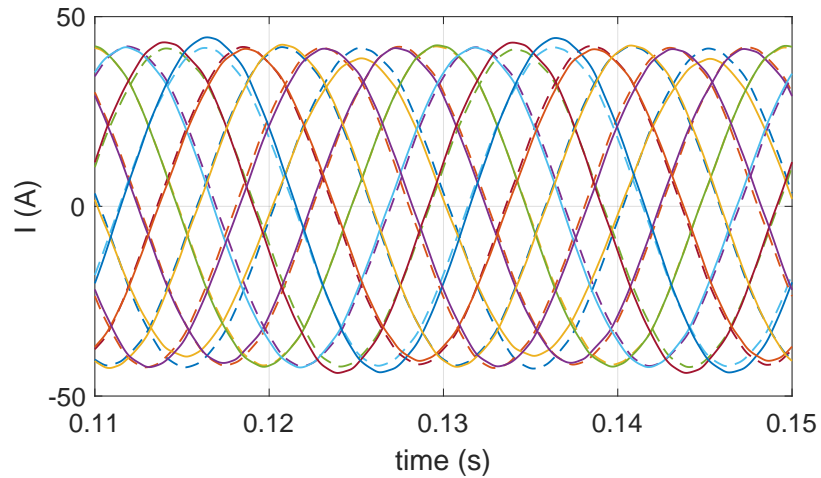

Figure 5: (Machine with an ASWC) 9 stator currents versus time in healthy (dashed lines) and faulty (solid lines, $R_{add} = 0.1\Omega$) states
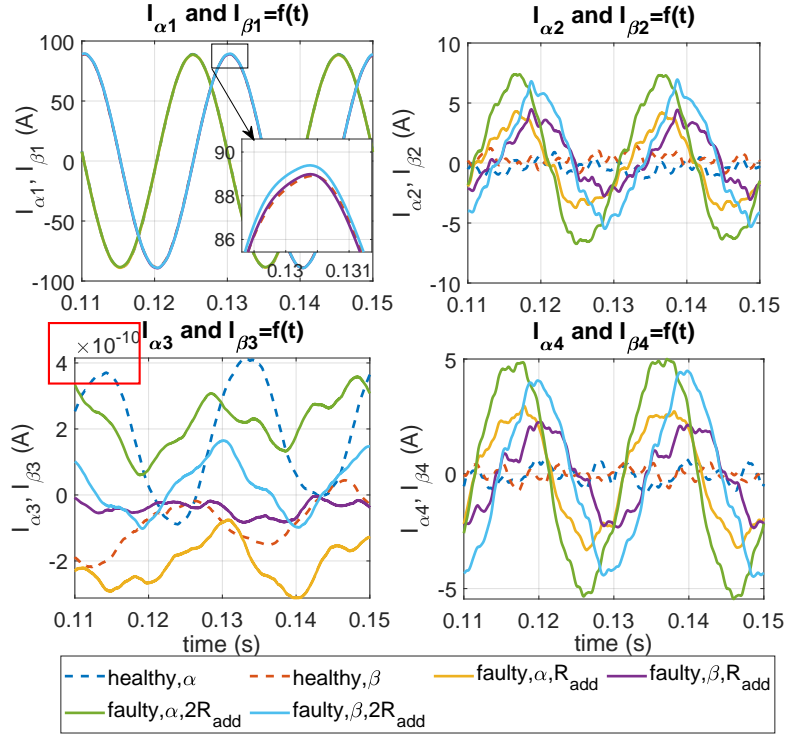
Figure 6: (Machine with an ASWC) Comparison of stator currents in $(\alpha_j, \beta_j), j \in \{1, 2, 3, 4\}$ subspaces in healthy and faulty ($R_{add} = 0.1\Omega$ then $2R_{add} = 0.2\Omega$) states: $I_{\alpha, \beta} = f(t)$

Figure 6 shows that the changes in $i_{\alpha_j, \beta_j} = f(t), j \in \{2, 4\}$ are much more significant. The currents in these two subspaces are very close to zero in the healthy state (dashed curves). When a fault occurs, they increase and their main component becomes the 1st order harmonic (solid curves). These changes give elliptical loci $i_{\beta_j} = f(i_{\alpha_j}), j \in \{2, 4\}$ (Figure 7). As shown in Table 2, the 1st order harmonic is not projected onto (α_2, β_2), (α_3, β_3) or (α_4, β_4) in the healthy state. When a fault occurs, this mapping is no more valid and all harmonics appear in all subspaces. More specifically, the 1st order harmonics appears in (α_2, β_2) and (α_4, β_4). Note that no changes are observed in (α_3, β_3) because of the 3 isolated neutrals that impose a null 3rd order harmonic current in both healthy and faulty states (8). In simulations, the currents in (α_3, β_3) are about 10^{-10} (A) due to some numerical errors.

$$\begin{cases} i_1 + i_4 + i_7 = 0 \\ i_2 + i_5 + i_8 = 0 \\ i_3 + i_6 + i_9 = 0 \end{cases} \tag{8}$$
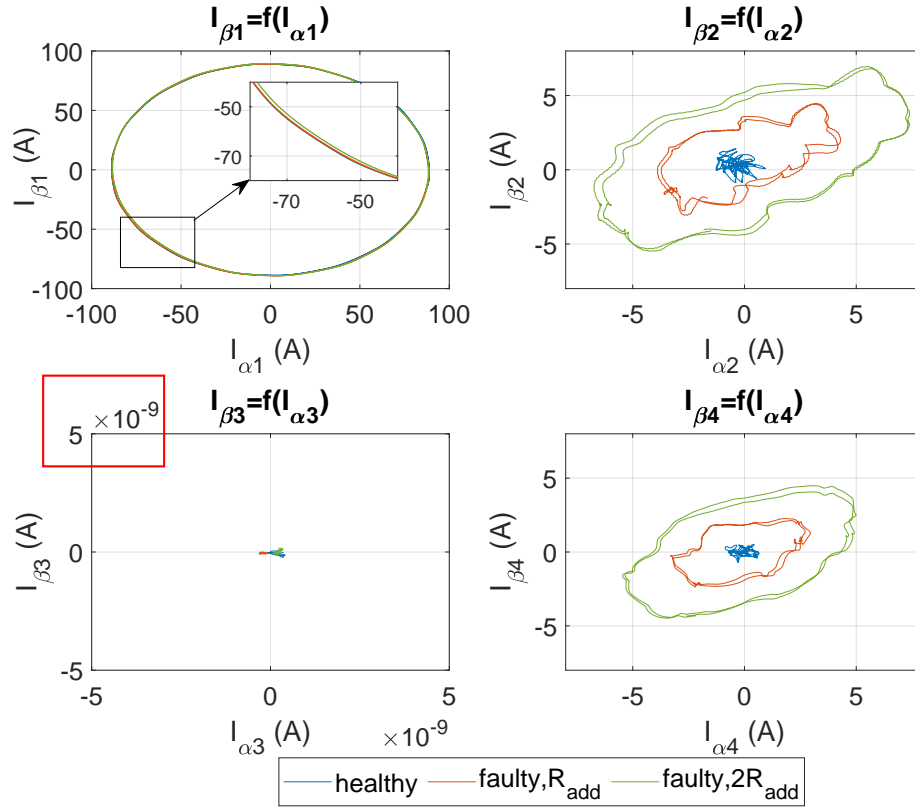
Figure 7: (Machine with an ASWC) Comparison of stator currents in (α_j, β_j) subspaces in healthy and faulty states with a variation of the severity of the fault $R_{add} = 0.1\Omega$ then $2R_{add} = 0.2\Omega$: $I_\beta = f(I_\alpha)$

By doubling the value of R_{add}, the different loci $i_{\beta_j} = f(i_{\alpha_j}), j \in \{2, 4\}$ get wider as shown in Figure 7. The fault $R_{add} = 0.1\Omega$ is then removed from phase 1 and added to phase 2. It is observed that the directions of the loci $i_{\beta_j} = f(i_{\alpha_j})$ change (Figure 8). Finally, the fault is added simultaneously on phases 1 and 2. The widths and the directions of the loci are different from those in the previous cases. Hence, it can be concluded that the variations of currents when projected onto (α_j, β_j) depend on the severity of the fault and its location. This shows that the chosen subspaces and quantities provide useful information for the elaboration of sensitive non-intrusive fault indicators.
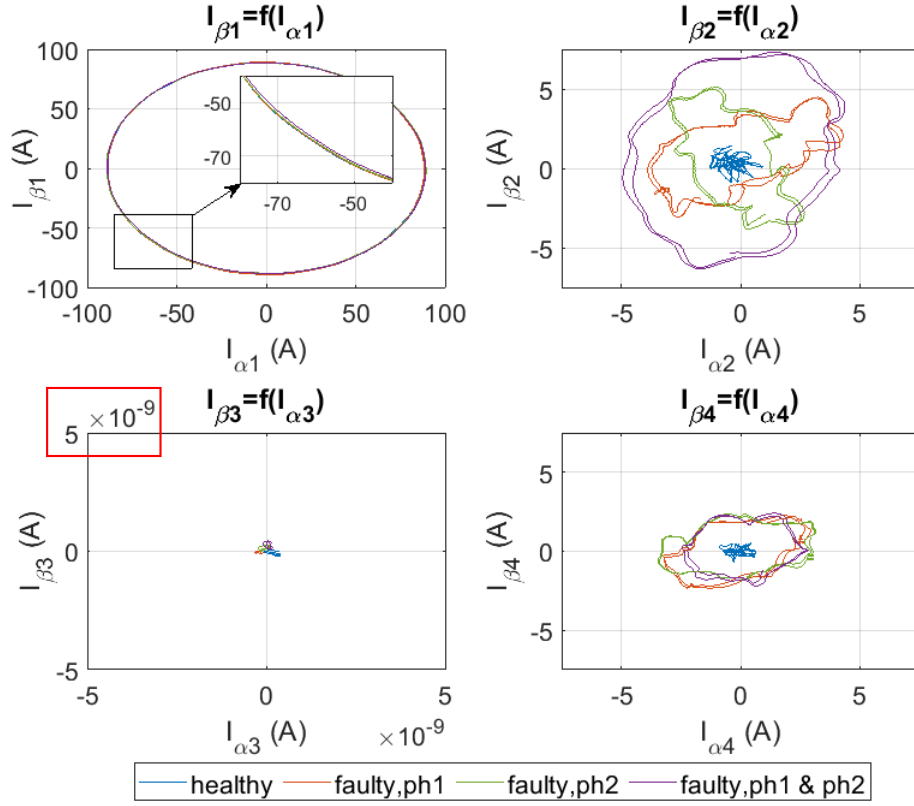
Figure 8: (Machine with an ASWC) Comparison of stator currents in (α_j, β_j) subspaces in healthy and faulty states with a variation of the location of the fault $R_{add} = 0.1\Omega$ on phase 1, $R_{add} = 0.1\Omega$ on phase 2, and $R_{add} = 0.1\Omega$ on phases 1 and 2: $I_\beta = f(I_\alpha)$

3.2. Comparison of phase currents in the rotating frame (d_j, q_j) in healthy and faulty states: machine with an ASWC

In the rotating frame (d_j, q_j), i_{d_j} and $i_{q_j}, j \in \{2, 4\}$ are nearly null in the healthy state. Only the (d_1, q_1) plane exhibits significant DC currents. The d_1 axis exhibits a null DC current, this is due to the MTPA control strategy. In the faulty state ($R_{add} = 0.1\Omega$, phase 1), the 1st order harmonic appears in (α_2, β_2) and (α_4, β_4) subspaces. The rotation angle in (d_2, q_2) being of $-7\theta_e$, 6th and 8th order harmonics appear in this subspace. Similarly, 4th and 6th order harmonics appear in (d_4, q_4) (rotation of $-5\theta_e$). The spectra of i_{d_j} and $i_{q_j}, j \in \{1, 2, 4\}$ are shown in Figure 9.

In the following subsection, it will be explained why fault signatures appear in phase currents, despite the current control. To do so, the interests of both Concordia and rotation transforms should be recalled.
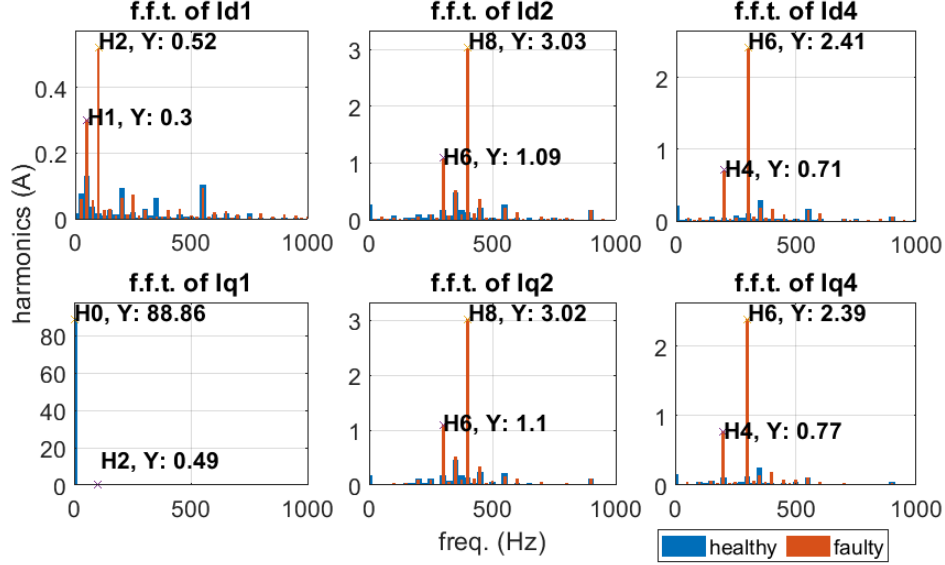
Figure 9: (Machine with an ASWC) Comparison of phase currents spectra in $(d_j, q_j), j \in \{1, 2, 4\}$ subspaces in healthy and faulty ($R_{add} = 0.1\Omega$, phase 1) states

3.3. Fault signatures in a closed-loop system

With MTPA control for non-sinusoidal PMSMs, the currents in the machine can be written as a sum of multiple harmonic currents [7, 10]. The control with PI of such a quantity is difficult and torque ripples may appear. By applying the VSD, each of the main harmonics ($1^{\text{st}}, 3^{\text{rd}}, 5^{\text{th}}$, and 7th order ones in the case of a 9-phase machine) is projected onto one (α_j, β_j) subspace and only one. Hence, sinusoidal quantities are obtained in the different (α_j, β_j) subspaces. To obtain constant quantities, one specific rotation per subspace (α_j, β_j) should be applied. The rotation angle depends on the main harmonic projected onto the given subspace.

For the 9-phase machine with an ASWC studied in this paper, rotations of θ_e, $-7\theta_e$, $3\theta_e$, and $-5\theta_e$ are respectively applied to (α_1, β_1), (α_2, β_2), (α_3, β_3), and (α_4, β_4). The subspaces of the rotating frame are noted $(d_j, q_j), j \in \{1, 2, 3, 4\}$. The stationary quantities can then be controlled with simple PI controllers, as long as four harmonics ($1^{\text{st}}, 3^{\text{rd}}, 5^{\text{th}}$, and 7th order ones) are sufficient for the characterization of the electromotive forces and the reference currents.

When a fault occurs, stator currents are no longer balanced and different harmonics appear in the different (α_j, β_j) subspaces. The control being based on the healthy operating mode, the transformation matrices and the controller parame-

ters are the same in both healthy and faulty states. Therefore, the projection of the phase currents onto the rotating subspaces results in oscillating quantities: DC component, 6th and 8th order harmonics in (d_2, q_2) and DC component, 4th and 6th order harmonics in (d_4, q_4). The signals in the feedback of the current loops are thus oscillating signals and the PI controllers, whose bandwidths are limited (90.7 rad.s^{-1} for the machine with an ASWC), do not compensate these oscillations, i.e. the fault signatures do not disappear. Note that if the current-controller bandwidth is increased, the effect of the fault on the currents is less significant, while the opposite trend is observed in the reference voltages [5]. The proposed fault detection strategy can therefore be applied on reference voltages.

4. Conclusions

In this paper, the impact of a resistance imbalance has been analysed for two nine-phase PMSMs with quite similar external characteristics but different winding arrangements. With the considered resistance imbalance, the impact on the phase currents, when plotted versus time, is almost invisible for both machines. However, the differences observed in the $(\alpha, \beta, 0)$ subspaces are significant. For the 9-phase machine with a symmetrical star winding configuration, the impact of a resistance imbalance in the space defined by $C_{9_{sym}}$ for decentralized d-q modelling is difficult to detect. On contrary, for the nine-phase machine with an asymmetrical star winding configuration, the impact of the imbalance in the space defined by $C_{9_{asym}}$ for VSD is quite visible. The detection of incipient resistance fault appears as easier for the asymmetrical configuration.

For future works, a diagnosis tool based on the relevant indicators presented above will be developed (as in [10]). To do so, several fault types and several severities should be considered and simulated. The ability of the indicators to discriminate between two different faults should also be analysed and proven.

References

[1] M. Cheng, Y. Zhu, The state of the art of wind energy conversion systems and technologies: A review, Energy Conversion and Management 88 (2014) 332–347.

[2] S. N. Foster, J. G. Cintron-Rivera, E. G. Strangas, Detection of incipient stator winding faults in PMSMs with single-layer fractional slot concentrated windings, Electric Power Systems Research 131 (2016) 231–243.

[3] R. Z. Haddad, C. A. Lopez, S. N. Foster, E. G. Strangas, A Voltage-Based Approach for Fault Detection and Separation in Permanent Magnet Synchronous

Machines, IEEE Transactions on Industry Applications 53 (2017) 5305–5314.

[4] R. Hu, J. Wang, A. R. Mills, E. Chong, Z. Sun, Detection and Classification of Turn Fault and High Resistance Connection Fault in Permanent Magnet Machines Based on Zero Sequence Voltage, IEEE Transactions on Power Electronics 35 (2020) 1922–1933.

[5] S. Huang, A. Aggarwal, E. G. Strangas, K. Li, F. Niu, X. Huang, Robust Stator Winding Fault Detection in PMSMs With Respect to Current Controller Bandwidth, IEEE Transactions on Power Electronics 36 (2021) 5032–5042.

[6] J. Hang, J. Zhang, S. Ding, M. Cheng, Fault Diagnosis of High-Resistance Connection in a Nine-Phase Flux-Switching Permanent-Magnet Machine Considering the Neutral-Point Connection Model, IEEE Transactions on Power Electronics 32 (2017) 6444–6454.

[7] M. Slunjski, O. Stiscia, M. Jones, E. Levi, General Torque Enhancement Approach for a Nine-Phase Surface PMSM With Built-In Fault Tolerance, IEEE Transactions on Industrial Electronics 68 (2021) 6412–6423.

[8] X. Kestelyn, E. Semail, Vectorial Modeling and Control of Multiphase Machineswith Non-salient Poles Supplied by an Inverter, in: Control of non-conventional synchronous motors, ISTE ; Wiley, London : Hoboken, NJ, 2012, pp. 161–206.

[9] E. Levi, FOC: Field-Oriented Control, in: Power Electronics and Motor Drives, CRC Press, 2011, pp. 6–15.

[10] M. Trabelsi, N. Nguyen, E. Semail, Real-Time Switches Fault Diagnosis Based on Typical Operating Characteristics of Five-Phase Permanent Magnetic Synchronous Machines, IEEE Transactions on Industrial Electronics (2016) 1–1.

[11] E. Levi, Multiphase AC Machines, in: J. Irwin (Ed.), Power Electronics and Motor Drives, CRC Press, 2011, pp. 6–21.

[12] M. Onsal, Y. Demir, M. Aydin, A New Nine-Phase Permanent Magnet Synchronous Motor With Consequent Pole Rotor for High-Power Traction Applications, IEEE Transactions on Magnetics 53 (2017) 1–6.

[13] E. Prieto-Araujo, A. Junyent-Ferre, D. Lavernia-Ferrer, O. Gomis-Bellmunt, Decentralized Control of a Nine-Phase Permanent Magnet Generator for Off-

shore Wind Turbines, IEEE Transactions on Energy Conversion 30 (2015) 1103–1112.

[14] A. Tani, L. Zarri, M. Mengoni, G. Serra, D. Casadei, Detection and localization of high resistance connections in quadruple three-phase induction motor drives, in: 2014 International Conference on Electrical Machines (ICEM), IEEE, Berlin, Germany, 2014, pp. 2094–2100.

[15] Y. Gritli, C. Rossi, G. Rizzoli, L. Zarri, A. Tani, D. Casadei, Detection and Localization of Incipient High Resistance Connection for Asymmetrical Twelve–Phase Induction Motor Drives, in: 2021 IEEE 13th International Symposium on Diagnostics for Electrical Machines, Power Electronics and Drives (SDEMPED), IEEE, Dallas, TX, USA, 2021, pp. 65–71.